Chemistry–A European Journal
Research Article
doi.org/10.1002/chem.202402600
Chemistry Europe
European Chemical Societies Publishing
www.chemeurj.org

Complex Biophysical and Computational Analyses of G-Quadruplex Ligands: The Porphyrin Stacks Back

Giuseppe Satta,[a, b] Marko Trajkovski,[c] Alessio Cantara,[d] Monica Mura,[e] Claudia Meloni,[e] Giulia Olla,[e] Michaela Dobrovolná,[d] Luisa Pisano,[a, b] Silvia Gaspa,[a] Andrea Salis,[e] Lidia De Luca,[a] Francesca Mocci,[e] Vaclav Brazda,[d] Janez Plavec,*[c, f, g] and Massimo Carraro*[a, b]

G-quadruplexes (G4 s), as non-canonical DNA structures, attract a great deal of research interest in the molecular biology as well as in the material science fields. The use of small molecules as ligands for G-quadruplexes has emerged as a tool to regulate gene expression and telomeres maintenance. *Meso*-tetrakis-(*N*-methyl-4-pyridyl) porphyrin (TMPyP4) was shown as one of the first ligands for G-quadruplexes and it is still widely used. We report an investigation comprising molecular docking and dynamics, synthesis and multiple spectroscopic and spectrometric determinations on simple cationic porphyrins and their interaction with different DNA sequences. This study enabled the synthesis of tetracationic porphyrin derivatives that exhibited binding and stabilizing capacity against G-quadruplex structures; the detailed characterization has shown that the presence of amide groups at the periphery improves selectivity for parallel G4 s binding over other structures. Taking into account the ease of synthesis, 5,10,15,20-tetrakis-(1-acetamido-4-pyridyl) porphyrin bromide could be considered a better alternative to TMPyP4 in studies involving G4 binding.

Introduction

Several genomic regions are characterized by a relative abundance of guanosine. The large amount of guanosine units, in the presence of monovalent cations such as K^+ and Na^+, allows their folding and leads to the formation of planar tetrads called G-quartets, together by a network of hydrogen bonds through Hoogsteen base pairing.[1,2] Stacking of G-quartets, stabilized by the coordination of the monovalent metal ion with the O6 oxygen of guanines, leads to the formation of "non-canonical" structures, characterized by a four chains helical structure, called G-quadruplexes (G4) (Figure 1a). The presence of G4 in telomeres and several other non-codifying regions of genome have been associated with a variety of regulatory

[a] G. Satta, L. Pisano, S. Gaspa, L. De Luca, M. Carraro
Department of Chemical, Physical, Mathematical and Natural Sciences, University of Sassari, Via Vienna 2, Sassari 07100, Italy
E-mail: mcarraro@uniss.it
[b] G. Satta, L. Pisano, M. Carraro
Consorzio Interuniversitario Reattività Chimica e Catalisi (CIRCC), Via Celso Ulpiani 27, Bari 70126, Italy
[c] M. Trajkovski, J. Plavec
Slovenian NMR Centre, National Institute of Chemistry, Ljubljana SI-1000, Slovenia
E-mail: janez.plavec@ki.si
[d] A. Cantara, M. Dobrovolná, V. Brazda
Institute of Biophysics, Czech Academy of Sciences, Královopolská 135, 612 65 Brno, Czech Republic
[e] M. Mura, C. Meloni, G. Olla, A. Salis, F. Mocci
Department of Chemistry and Geological Science, University of Cagliari, Cittadella Universitaria, I-09042 Monserrato, Italy
[f] J. Plavec
EN→FIST Centre of Excellence, Trg OF 13, SI-1000 Ljubljana, Slovenia
[g] J. Plavec
Faculty of Chemistry and Chemical Technology, University of Ljubljana, Vecna pot 113, SI-1000 Ljubljana, Slovenia

Supporting information for this article is available on the WWW under https://doi.org/10.1002/chem.202402600

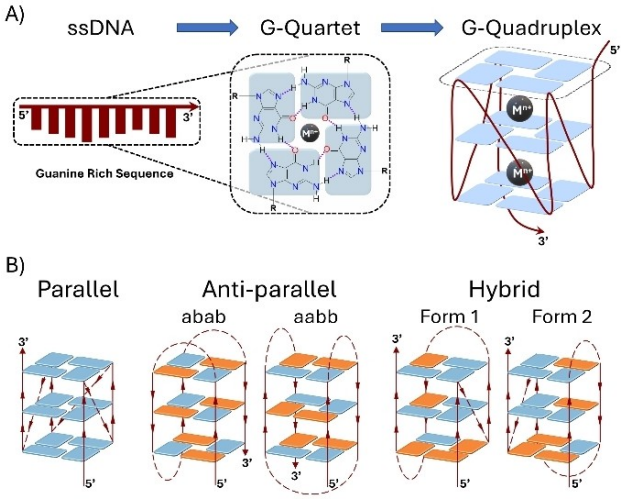

Figure 1. (A) structure of the G-quartet formed by Hoogsteen base pairing of four guanine residues and piling up to give G4. (B) Schematic intramolecular topologies of G4 structures. Blue and orange rectangles depict guanines exhibiting *syn* and *anti* conformation of glycosidic torsion angle, respectively. In the case of antiparallel topology, *a* and *b* denote the orientations of the G-tracts, corresponding to upward and downward directions, respectively, starting from the 5′ end in a clockwise manner.

functions. The human telomere is approximately 5,000 to 8,000 base pairs in length and features a single-stranded 3′ overhang ranging from 100 to 200 bases.[1] This overhang is primarily composed of the repetitive TTAGGG sequence. Most healthy cells possess a limited capacity for division, as was demonstrated by Hayflick and Moorhead in 1961.[3] It is currently known that this effect is related to telomere length, which act as biological clocks that, after reaching a limiting length, trigger the senescence process.[4] A problem often correlated with the presence of tumor activity is abnormal cellular proliferation, which in most cases, is associated with the overexpression of telomerase activity.[5] This enzyme, a reverse cellular transcriptase, regulates telomere elongation, thereby preserving its integrity. A correlation has been assessed between telomere length maintenance and the cellular ability, typical of cancer cells, to escape replicative senescence, and in fact more than 90 percent of cancer cells show telomerase enzyme activity.[6] The fact that most healthy cells are telomerase-silent while there is its overexpression in cancer cells, makes this enzyme an attractive target for post-diagnosis treatments. The inhibition of telomerase can be achieved either through small molecules that bind directly to the enzyme[7,8] or by stabilizing G4 structures. The latter method involves the use of ligands that bind to and stabilize G4 structures, which act as physiological blocks to the telomerase's ability to code and extend telomeres.[9] G4 can also be found in oncogene promoters, replication initiation sites and untranslated regions, showing their biological relevance.[10–12] For example, the c-Myc gene plays an essential role in the regulation of cell growth, proliferation, and apoptosis. When over-expressed or mutated, as in cancer cells, this gene can drive cells toward uncontrolled proliferation and thus contribute to the formation of various types of cancer.[13] Within its sequence, the c-Myc proto-oncogene possesses the nuclear hypersensitivity element III_1 ($NHEIII_1$) region which has been shown to be highly influential in the regulation of this gene.[14] Stabilizing this structure with ligands was noted to suppress further transcriptional activation of the c-Myc gene.[15] G4 can be unimolecular or intermolecular. Depending on the orientation of the chains, they can adopt different topologies[16] (Figure 1b), influenced by factors such as molecular crowding[17,18] and nature of monovalent cation.[19] Furthermore, the structural and biochemical features of G4 s, prompted their use in biosensors[20] and nanomaterials.[21,22]

The study of G4 ligands has thus become a productive field of research.[23–32] Basically, there are 4 ways in which a ligand can interact with a G4: stacking on top or bottom G-quartets, intercalation between them, interaction with loops, or a combination of these ways. Electron-deficient cores promote interactions through π-π stacking, while cationic portions on substituents determine electrostatic interactions with negative charged phosphodiester groups, and so on.[33] These considerations led to the discovery of various types of ligands, among others porphyrins: natural derivatives include Fe(III)-protoporphyrin IX,[34] while the first synthetic derivative is 5,10,15,20-tetrakis-(N-methyl-4-pyridyl)porphyrin (**TMPyP4**), whose activity as telomerase inhibitor was demonstrated by Wheelhouse et al. in 1998.[35] **TMPyP4** has been shown also to reduce the expression of the proto-oncogene c-Myc and several c-Myc-regulated genes that contain G4-forming sequences. This modulation led to in vivo antitumor effects in various models, including the ability to inhibit tumor growth and prolong survival.[36] **TMPyP4**, has become a staple between ligands used in G4 studies but displayed a limited selectivity,[37] prompting to the development of various derivatives with demanding synthesis.[38–41] In this work, several simple porphyrin derivatives with potential binding and stabilizing activity toward G4 were screened through a molecular modelling procedure, which included docking and molecular dynamics. Simulations were conducted on different G4 s comprising one from the human telomeric sequence with a parallel topology (PDB ID:1KF1[42]) and another present in the $NHEIII_1$ region of the c-Myc proto-oncogene, also known to have a parallel propeller type topology (PDB ID: 1XAV[43]). The results of the docking procedure guided in the choice of the derivatives to be synthesized and subjected to various stability and binding studies. Specifically, a derivative of 5,10,15,20-tetrakis-4-pyridyl-porphyrin (**TPyP**) with amidomethyl substituent was found to be the most promising, and its properties are here compared with those of well-known porphyrin derivative, **TMPyP4**. One of the focuses of the work was to assess whether substituting the methyl groups of **TMPyP4** affect its interaction with G4 from telomere and c-Myc. This comparison was made by evaluating the results obtained for the substituted derivatives alongside those obtained for **TMPyP4** using NMR spectroscopy and mass spectrometry. NMR spectroscopy has proven to be a very versatile technique for assessing the formation of a complex, and providing crucial insights into the mode of ligand/G4 interaction. In particular NOESY and ROESY experiments,[43–45] have been employed for structural assessment of the complexes and identification of the corresponding G4-ligand interfaces. The stability of the ligand/G4 complexes was evaluated by mass spectrometry,[46–48] specifically, with MS/MS technique: the intensity of isolated molecular ion generated by the porphyrins/G4 complex was measured as a function of increasing collision energy in the analyzer. Porphyrin derivatives were then subjected to some preliminary tests to evaluate their cytotoxicity on breast cancer (MCF-7).

Results and Discussion

In this work, the interaction between tetracationic porphyrins derivatives and different DNA G4 s was evaluated. Proposed ligand structures, based on the porphyrin core (Figure 2) with different meso substituents, are reported in Table 1. **TMPyP4**, chosen as literature reference ligand, and designed ligands, **PL1** to **PL7**, were first subjected to molecular docking calculations on different G4 structures. Most promising ligands were then synthetized, and their G4 binding abilities studied by UV and NMR spectroscopies and mass spectrometry. Chosen sequences were derived from the $NHEIII_1$ region of the c-Myc proto-oncogene, and the human telomeres.

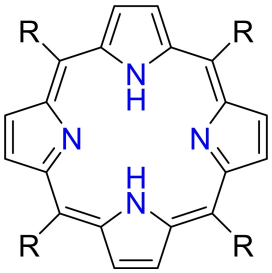

Figure 2. Porphyrin general core. R groups indicate *meso* substituents.

Table 1. Proposed porphyrin ligands' meso substituents.

Ligands	Ligands' *meso* substituents (R)	MW
TMPyP4	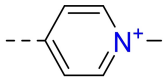	678.84
PL1	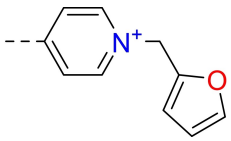	943.07
PL2	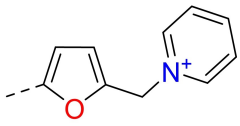	943.07
PL3	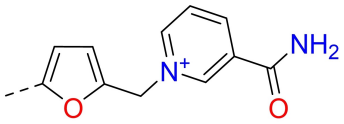	1115.75
PL4	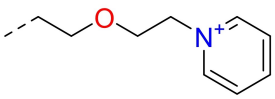	911.16
PL5	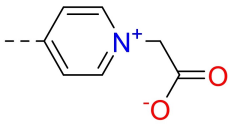	850.83
PL6		907.05
PL7		850.94
PL7-Me	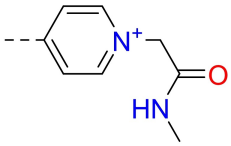	907.05
PL7-2Me	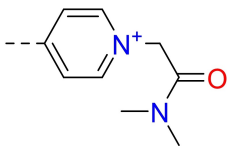	963.16

Molecular Docking

The GScore values for the best poses obtained for the studied ligands on the studied G4 s are reported in Table 2. According to the docking results obtained on all-parallel G4 1XAV and 1KF1, candidates **PL3**, **PL6** and **PL7** were the most promising. Unfortunately, the synthesis of **PL3** proved to be challenging. Given that **PL6** and **PL7** exhibited a comparable G4 affinity to that showed by **PL3**, the synthesis of the latter was not pursued further. It was observed that both **PL6** and **PL7** demonstrated binding ability to other topologies in addition to the all-parallel ones. However, given the absence of stereocenters and the lower molecular weight, **PL7** was selected for further computational studies.

Molecular Dynamics Simulations

To investigate the impact of **PL7** on the stability of G4, a series of molecular dynamics (MD) simulations were conducted. The system was simulated in a water solution using 1KF1 as G4, both in the presence and absence of the ligand. For the complex **PL7/G4**, the structure obtained from molecular docking studies was used. Simulations were conducted at temperatures of 300, 500, 525 and 550 K, to induce denaturation. Experimentally, the process of thermal denaturation is observed to occur over a timescale that is too long to be replicated within the constraints of reasonable timescales in silico. The use of higher temperatures than those measured in real laboratory experiments has been found to accelerate the denaturation process and make it occur within accessible timescales for MD simulations.[49–51] It is important to note that this approach is feasible due to the harmonic potentials of the force field, which prevent significant deviations in bond length or bond breakage even at elevated temperatures. Furthermore, previous studies have demonstrated that increasing temperature does not alter the denaturation pathway.[49,50] This strategy has recently been employed to assess the stabilization of the G4 structure following interaction with ligands, with results that are consistent with experimental data.[52] Figure 3 presents the root-mean-square deviation (RMSD) values calculated for the entire G4 structure, its complex with **PL7**, and selected portions during the MD simulation performed at 300 K. To ascertain the stability of the **PL7**/**1KF1** complex, both the DNA atoms (shown in blue) and the ligand atoms (shown in yellow) were considered in RMSD simulations. The matching of the two RMSD values indicated that the ligand, once it was bounded, did not move significantly from its initial position, remaining stably linked to the G4. Moreover, the comparison of the RMSD between the free 1KF1 and **PL7**/**1KF1** indicated that the ligand induced stabilization, as evidenced by the slightly smaller RMSD values in its presence.

This stabilization could be primarily attributed to the enhanced stability of the loops. The simulations at higher temperatures confirmed the stabilization effect of the ligand, as shown by the RMSD of the simulations performed at 525 K, shown in Figures 3D and E. As expected, the RMSDs of the

Table 2. GScore results from molecular docking experiments.

Ligands	1XAV[a]	1KF1[b,f]	2JPZ[c]	2HY9[d]	143D[e]
TMPyP4	−13,50	np[g]	np	np	np
PL1	−14,11	−14,63	-[h]	-	np
PL2	−14,77	−14,16	-	-	−12,79
PL3	−17,84	−19,14	-	-	−14,70
PL4	−9,89	−15,77	-	-	np
PL5	−14,07	−14,28	np	−14,09	-
PL6[j]	−17,74	−19,12	−15,29	−15,36	-
PL7	−18,69	−18,66	−18,21	−16,79	−14,81

G4 names correspond to PDB ID. [a] Main G4 forms in the c-MYC promoter gene. [b] Human telomeric parallel G4. [c] Human telomeric hybrid-form 1 G4. [d] Human telomeric hybrid-form 2 G4. [e] Human telomeric antiparallel G4. [f] All G4 structures were determined in solution by NMR except for 1KF1 (X-Ray solid structure). [g] np: no poses were found. [h] the dash symbol indicates that the docking was not performed. [j] Configuration of the chiral centers of ligand PL6 in the best pose: SRSR, SSSS, SRRS, SSSS.

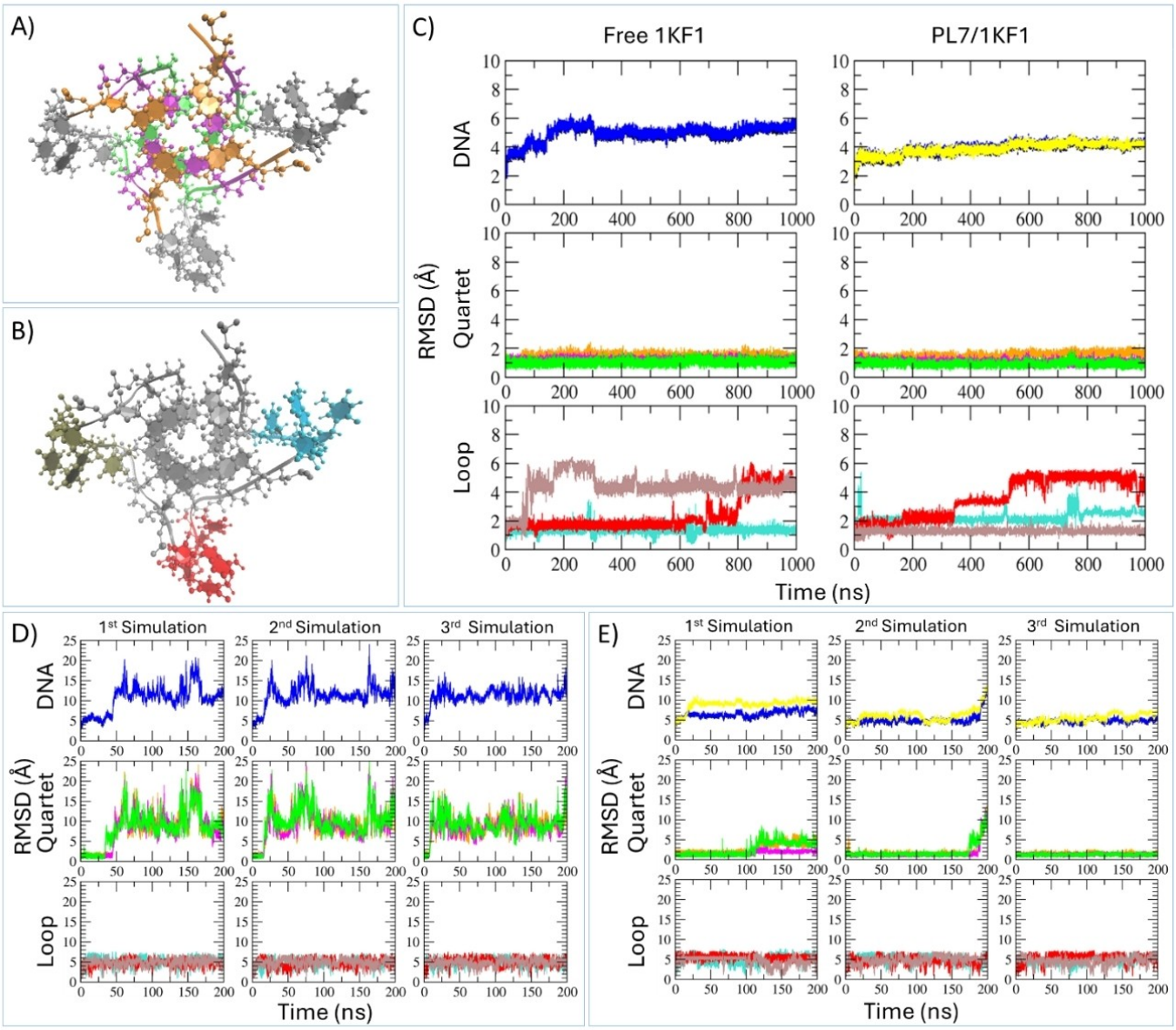

Figure 3. RMSD Results. (A)Color code used for quartets (B) Color code used for loops. These colors are the same used to indicate RMSD values. (C)RMSD calculated on: (top row) 1KF1 atoms except the first base in the 5′ direction (blue), and PL7/1KF1 atoms (yellow); (middle row) on each of the three G-quartets; (bottom row) on each of the three loops. Simulations conducted at 300 K. (D) RMSDs calculated on three separate simulations at 525 K of free 1KF1. (E) RMSDs calculated on three separate simulations at 525 K of PL7/1KF1.

system at 525 K were in general higher than those at 300 K, however the behavior with and without the ligand was qualitatively very different. The RMSD of the loops revealed that these flexible portions did not keep their original organization at high temperature, either in absence or in presence of the ligand. However, the ligand had a strong effect on the stability of the G-quartets: in free 1KF1, denaturation occurred within the first 50 ns. In the presence of PL7, denaturation was slower or not reached at all (Figure 3E - middle row), keeping the G4 structure stable. The simulations performed at 500 K and 550 K confirmed the stabilizing effect of the ligand, as shown by the RMSD reported Figure S3.

Synthetized Oligonucleotides

The sequences used in the docking studies were taken as a starting point for choosing those to be used in the spectroscopic and spectrometric studies (Table 3). The sequence indicated by the acronym 23TAG (PDB ID: 2JSK[53]) has been employed, corresponding to tandem repeats of the human telomeric region. This sequence in K^+ solution leads to the folding of a form1/form2 hybrid topology G4, with a 70:30 ratio respectively.[54] On the other hand, the modified sequences reported as CMA (PU19-A2 A11,[55] PDB ID:2LBY) and CMT (PU19-T2 A11[55]) are derived from the first 4 of 5 guanosine domains present in the $NHEIII_1$ region of the c-Myc gene.[44] CMA and CMT tend to fold in parallel topology G4 in a K^+ solution. This enabled the assessment of both the binding capacity and the selectivity of the proposed ligands toward G4 structures with different topologies.

Table 3. DNA oligonucleotide sequences used in this study.

		1	2	3	4	5	6	7	8	9	10	11	12	13	14	15	16	17	18	19	20	21	22	23	
23TAG	5′-	T	A	G	G	G	T	T	A	G	G	G	T	T	A	G	G	G	T	T	A	G	G	G	-3′
CMA	5′-	T	A	G	G	G	A	G	G	G	T	A	G	G	G	A	G	G	G	T					-3′
CMT	5′-	T	T	G	G	G	A	G	G	G	T	A	G	G	G	A	G	G	G	T					-3′

DNA oligonucleotides were synthesized on DNA/RNA H-8 Synthesizer using standard phosphoramidite chemistry with DMT protecting group

Binding Constant UV-Visible Evaluation

UV-visible spectra of solutions of **TMPyP4** and **PL7** (Figure S8) were recorded upon addition of calf thymus DNA, 23TAG, and CMA, at 25 °C within the wavelength range of 200–800 nm. The porphyrins spectra typically exhibited a Soret band around 428 nm. Upon addition of DNA, in the **TMPyP4** solution, a red shift of the maximum absorption band was observed for the duplex, 23TAG, and CMA, with shifts of 2.3 nm, 2.1 nm, and 2.9 nm, respectively. Similarly, the red shifts observed for the **PL7** spectra amounted to 0.8 nm with duplex, 9.7 nm with 23TAG, and 5.8 nm with CMA. This red shift phenomenon can be associated with a decrease in the energy of the $\pi \rightarrow \pi^*$ transition due to the interaction between the π-bonding orbital of the DNA base pairs and the empty π^*-antibonding orbital of the ligand. The hypochromic effect, determined by comparing absorbance maxima, was evidence of the interaction occurring between the nucleotides and porphyrins. The hypochromic effect (Table 4) increased in the order duplex < 23TAG < CMA with **TMPyP4** and in the order duplex < CMA < 23TAG with **PL7**, showing a difference compared to the duplex titration, of +9% (TAG23) and +5% (CMA). Binding constants could be determined by applying Benesi-Hildebrand method as reported in Supporting Information. The obtained values aligned with those

Table 4. Red shift and hypochromicity.

	TMPyP4		PL7	
	△λ (nm)	△A (%)	△λ (nm)	△A (%)
Duplex	2.3 ± 0.1	18 ± 2	0.8 ± 0.2	30 ± 2
23TAG	2.1 ± 0.4	22 ± 1	9.7 ± 0.5	39 ± 3
CMA	2.9 ± 0.5	24 ± 1	5.8 ± 0.3	35 ± 2

Calculated at Soret band by titrating 5 μM porphyrin with 0.5 μM DNA. DNA solutions were prepared in a 20 mM potassium phosphate buffer at pH 7 and stored at 25 °C with slow rotation for 24 hours. Calf thymus DNA was used as a reference for duplex DNA. Porphyrin solutions at were prepared in the same buffer. Each experiment was repeated from 3 to 5 times, and the results are presented as the mean ± standard deviation.

documented in the literature.[56,57] While **TMPyP4**, employed as a reference due to its well-established status, demonstrated binding constant values consistent across all studied DNA types ($1.1–1.5\times10^6$ M^{-1}), **PL7** exhibited selectivity for the CMA sequence over the duplex, displaying a binding constant 2.6 times higher (Table 5).

NMR Study of Complex Structures

To assess interactions of herein synthesized porphyrin analogues with G4, ^{1}H NMR monitored titration of 23TAG and CMA G4 s were performed. These oligos differ slightly from the wild-type segments in order to increase the NMR spectral resolution in the imino-proton region without affecting the native structure. Notably, our studies were conducted in aqueous solutions at 20 mM K-phosphate, excluding KCl that reduces solubility of the herein studied porphyrin derivatives. Importantly, the acquired ^{1}H NMR spectra of CMA and 23TAG folded in 20 mM K-phosphate without KCl, match literature reported spectra of G4 folded in the presence of 70/100 mM KCl.[44,54,58,59] ^{1}H NMR spectrum of CMA at 20 mM K-phosphate exhibits twelve imino signals in the range from δ 11.04 to 12.06 ppm, consistent with the formation of G4 with three G-quartets, i.e. G3→G7→G12→G16, G4→G8→G13→G17 and G5→G9→G14→G18, each comprising four Hoogsteen-type hydrogen-bonded guanine residues. Notably, the parallel-stranded topology of (free) CMA G4 relates to the core of the structure comprising guanine residues, which are connected with two single-residue (T6 and T15) and one two-residue (T10-A11) propeller-type loops, while overhangs on 5′- and 3′-ends consist of A1-T2 and T19, respectively. Upon addition of 0.5 mole equivalents of **PL7** the imino ^{1}H NMR signals corresponding to the 'free CMA G4' became less intense and a new set of signals was observed in the range between ^{1}H δ 10.08 and 11.02 ppm (Figure 4B).

The new set of signals intensified at 1:1 ratio of DNA: Ligand, consistent with the formation of a 1:1 binding stoichiometry complex called 'Complex a'. Moreover, at the equimolar concentrations of DNA and ligand there was an equilibrium between 'free CMA G4' and 'Complex a' in a slight preference of the latter, while the species were in slow exchange on the ^{1}H NMR timescale at 600 MHz. ^{1}H NMR spectral analysis at 1.5 mole equivalents of **PL7** shows that intensity of signals corresponding to 'free CMA G4' decreased, while the 'Complex a' persisted as the predominant species. NOESY and ROESY spectral analysis conducted at 1:1 DNA:ligand binding stoichiometry revealed cross-peaks arising from chemical exchange between 'free CMA G4' and 'Complex a', enabling assignment of new CMA imino chemical shifts influenced by the proximity of **PL7** (Figure 5 and Figure S5). Furthermore, comparison of imino ^{1}H NMR chemical shifts of free CMA G4 and 'Complex a' showed the largest perturbations for guanine residues at the 5′-end G-quartet, i.e. G3→G7→G12→G16, and the smallest for G5→G9→G14→G18 quartet at the 3′-end (Figure 5 and Figure S6). These results are consistent with 'Complex a' corresponding to CMA G4 exhibiting **PL7** stacked

Table 5. Binding constants of porphyrins with duplex and G4 DNA sequences.

	K_b (M^{-1})	
	TMPyP4	PL7
Duplex	$(1.1 \pm 0.8)\times10^6$	$(6.5 \pm 0.1)\times10^5$
23TAG	$(1.5 \pm 0.4)\times10^6$	$(6.1 \pm 0.3)\times10^5$
CMA	$(1.5 \pm 0.6)\times10^6$	$(1.7 \pm 0.4)\times10^6$

The Benesi-Hildebrand method was used to calculate the binding constant (K_b)

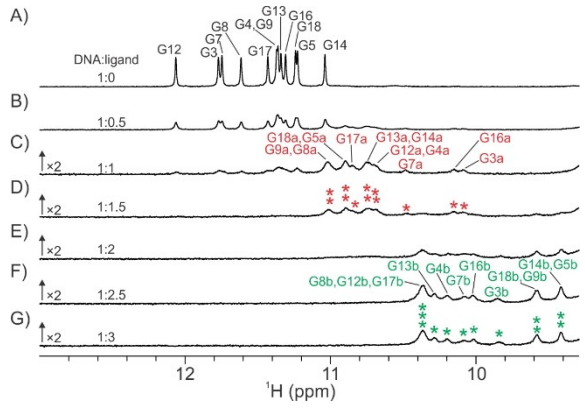

Figure 4. Imino region of the ^{1}H NMR spectra of CMA G4 upon titration with PL7, whereby the molar ratios of DNA and the ligand are indicated above corresponding spectra. The signals corresponding to the 'free CMA G4', 'Complex a' and 'Complex b' are indicated with black, red, and green colors, respectively. Spectra were recorded at 0.2 mM DNA concentration, 25 °C in 90 %/10 % $H_2O/^2H_2O$, at 20 mM KPi, pH 7.0.

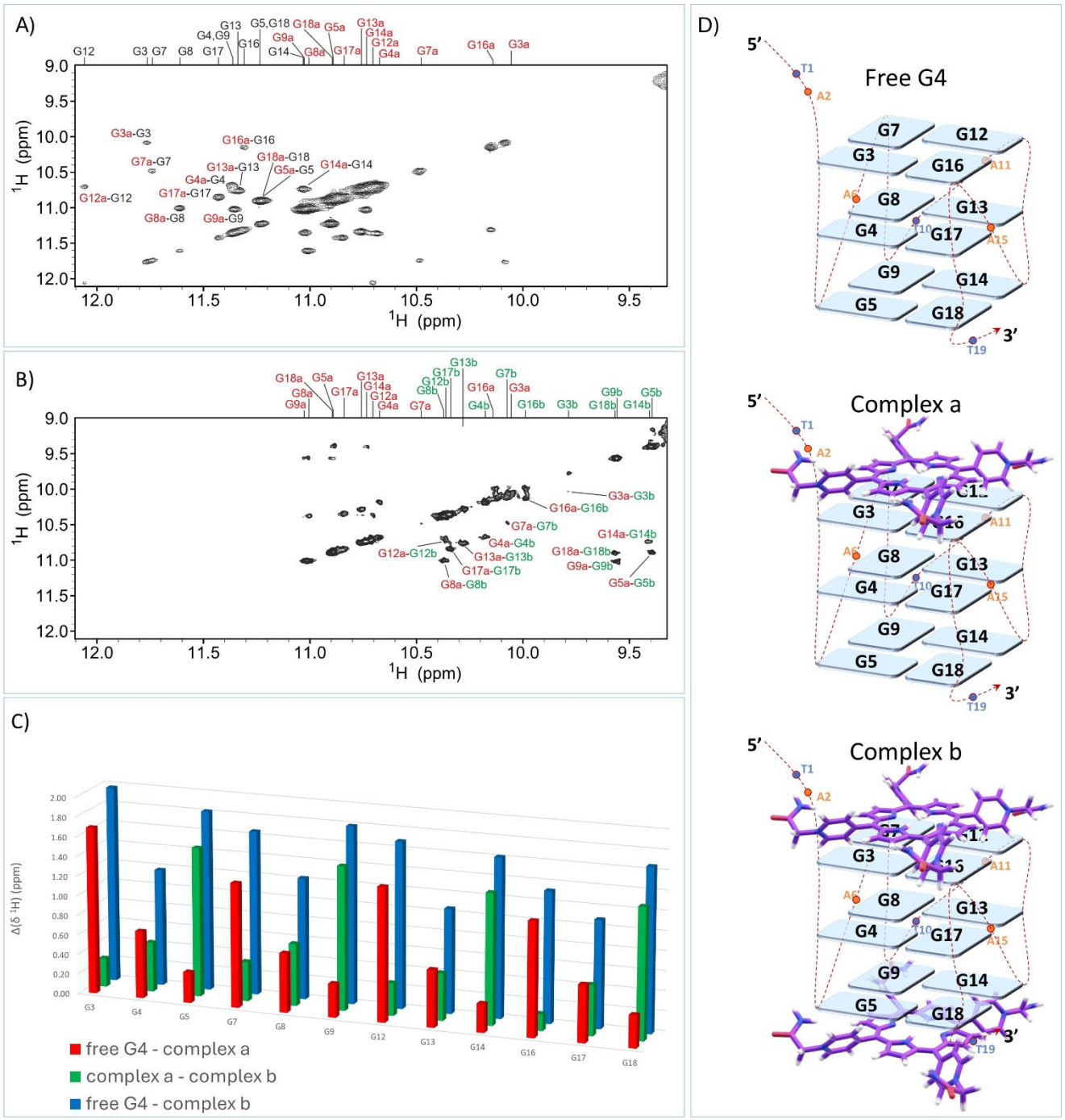

Figure 5. Imino–imino region of NOESY spectra (τm = 200 ms) of CMA in the presence of A) 1 and B) 2 mole equivalents of PL7 with indicated cross-peaks corresponding to chemical exchange A) between 'free CMA G4' and 'Complex a'; B) between 'Complex a' and 'Complex b'. Imino ^{1}H NMR chemical shifts corresponding to the 'free CMA G4, 'Complex a' and 'Complex b' are labelled in black, green, and red, respectively. The spectra were recorded at 0.2 mM DNA concentration, 25 °C in 90%/10% $H_2O/^2H_2O$, at 20 mM KPi, pH 7.0. C) Imino ^{1}H NMR chemical shift changes induced by interaction of CMA G4 and PL7, whereby red, green, and blue bars indicate Δ(δ^1H) between 'free CMA G4' and 'Complex a'; between 'Complex a' and 'Complex b'; between 'free' CMA G4 and 'Complex b', respectively. D) Schematic depiction of 'free CMA G-quadruple' (top), of the 'Complex a' corresponding to CMA G4 exhibiting the ligand bound at its 5′-end G-quartet (middle) and 'Complex b' corresponding to CMA G4 exhibiting two ligands bound to G-quartets, i.e. 5′- and 3′-end (bottom).

on the G3→G7→G12→G16 quartet and positioned proximal to the 5′-end overhanging residues T1 and A2 (Figure 5D). This was corroborated also by the observed ^{1}H NMR chemical shifts changes upon formation of 'Complex a' that were around 1.0 ppm for the methyl groups of T1 (located at the 5′-end). The fact that DNA-ligand NOE interactions were not resolved suggests that the binding was dynamic and involved exchange of the ligand between free- and bound-state and/or ligand reorientation at the binding site. Interestingly, at 2 mole equivalents of **PL7** ^{1}H NMR signals corresponding to 'Complex

a′ were reduced, while yet another set of signals appeared between ^{1}H δ 9.4 and 10.4 ppm in line with the formation of 'Complex b', wherein CMA G4 and **PL7** interacted at 1:2 binding stoichiometry (Figure 4E). ^{1}H NMR signals corresponding to 'Complex b' were further intensified at 2.5 mole equivalents of **PL7**, while precipitate was observed in the NMR sample at 3 (and higher) mole equivalents of the ligand with respect to 0.2 mM DNA, thus precluding further titration experiments. Notably, the slow exchange of 'Complex a' and 'Complex b' observed at 2 mole equivalents of **PL7** enabled identification of the corresponding NOESY and ROESY cross-peaks resulting from chemical exchange (Figure 5 and Figure S5). The analysis enabled assignment of imino ^{1}H NMR chemical shifts of CMA G4 within 'Complex b', furthermore allowing ^{1}H NMR chemical shift perturbation analysis showing that the 'Complex b' resulted upon **PL7** binding to the G5→G9→G14→G18 quartet at the 3′-end of the CMA G4 comprised in 'Complex a' (Figure 5D). In detail, comparison of imino ^{1}H NMR chemical shifts of 'Complex b' and 'Complex a' showed the largest differences for G5→G9→G14→G18 quartet at the 3′-end of the CMA G4, while the smallest ones for G3→G7→G12→G16 quartet at the 5′-end of the CMA G4. On the other hand, the Δ(δ ^{1}H) for imino signals of 'Complex b' with respect to those for 'free CMA G4' showed that differences were similar for the G3→G7→G12→G16 and G5→G9→G14→G18 quartets, in line with **PL7** stacked on both. Altogether, the NMR data were consistent with moderate to strong binding of **PL7** to CMA G4, whereby interactions comprised stacking of the ligand to the outer G-quartets, of which the 5′-end represented the preferential binding site.

Similar ^{1}H NMR studies were also extended to derivatives **PL7-Me** and **PL7–2Me** (Table 1), in which the amide hydrogens were replaced with 1 or 2 methyl groups respectively, to evaluate whether these structural modifications could modulate their interaction capabilities. Study of interactions of CMA G4 with **PL7-Me** and **PL7-2Me** relied on the use of 1D and 2D NMR experiments analogous as described above for **PL7** (Figure S4). Upon addition of 0.5 to 1.5 molar equivalents of **PL7-Me** and **PL7-2Me** with respect to DNA, the ^{1}H NMR signals corresponding to ′free CMA G4′ gradually became less intense and, in turn, a new set of signals was observed, consistent with the formation of ′Complex a′ with ligand bound to the 5′ end of CMA G4. Furthermore, no signals corresponding to DNA-ligand interactions were identified, whereas cross-peaks were observed in NOESY and ROESY spectra consistent with chemical exchange between ′free CMA G4′ and ′Complex a′. Preferential binding of **PL7-Me** and **PL7-2Me** to the G3→G7→G12→G16 quartet is inferred from analyses of imino ^{1}H NMR chemical shift perturbation (Figure S6). Further additions to 2, 2.5 and 3 mole equivalents of **PL7-Me** or **PL7–2Me** with respect to CMA resulted in conversion of 'Complex a' into 'Complex b', in which ligands stacked at both outer G-quartets of CMA G4 as inferred from the observed ^{1}H NMR chemical shift perturbations (Figure S6 and Table S1). Comparison of the ^{1}H NMR imino-protons chemical shift perturbations of CMA G4 upon binding of tetra-substituted porphyrins with different pendant groups showed very similar profiles, i.e. insignificant differences between **PL7** and **PL7-Me**, while slight variations were observed in the case of **PL7-2Me**. Most notable differences in ^{1}H NMR chemical shifts were observed when comparing 'Complex b' for **PL7–2Me** with respect to **PL7** and **PL7-Me**. Furthermore, the imino protons of G3, G7, G12, and G16 were shifted up field with Δδ of 0.24, 0.15, 0.19, and 0.25 ppm for **PL7-Me** vs. **PL7-2Me**; this suggests that dimethylamide groups in **PL7-2Me** slightly interfered with G4 binding, probably by sterically hindering ligand interactions at the binding site comprising the 5′-end G3→G7→G12→G16 quartet. Considering that the G4 exhibits two 5′-end residues (T1-A2) while only one residue at the 3′-end (T19) where the preference of **PL7-2Me** binding is rather similar to **PL7** and **PL7-Me** suggests that binding relies not only on stacking of the ligands to G-quartets, but also on interactions between the ligand's pedant groups and overhanging residues. Consistent with this, extending the comparative analysis of ^{1}H NMR chemical shift perturbations to include NMR data on the binding of CMA G4 to the reference compound TMPyP4 (characterized by the shortest substituent on the pyridine nitrogen atom) showed that it bound slightly more strongly than **PL7**, **PL7-Me**, and **PL7-2Me** (Figure S6). To further explore binding of the herein studied porphyrin derivatives to G4 exhibiting different topologies ^{1}H NMR-monitored titration was performed on 23TAG, which at 20 mM KCl adopts G4 with hybrid-1 type topology while upon molecular crowding conditions induced by DMSO refolds into parallel-stranded G4.[18] At diluted conditions and in the absence of ligand, ^{1}H NMR spectrum of 23TAG exhibited twelve major signals in the imino region characteristic for Hoogsteen-hydrogen bonded guanine residues, consistent with formation of the predominant G4 exhibiting hybrid type-1 topology (Figure S8 A). Additional broader ^{1}H NMR imino signals were observed corresponding to minor G4 forms present in the equilibrium. The ^{1}H NMR imino signals for both, the major and minor G4 forms decreased upon addition of 0.5 mole equivalent of the **PL7**. This effect was pronounced gradually at equimolar DNA and ligand concentrations as well as along the course of titration, whereby at 3 mole equivalents of the **PL7** most of the signals corresponding to the initial G4 were broadened almost to the baseline. In parallel, formation of DNA-ligand complex(es) was indicated by the new set of ^{1}H NMR signals appearing at 1:1 ratio. However, the signals corresponding to the complex remained weak/broad even at 1:1.5 and 1:2 ratio of DNA to ligand, suggesting weak, or at most moderate binding that resulted in an equilibrium of free 23TAG G4 and complexes with non-specifically bound **PL7**. In the solution mimicking molecular crowding conditions a single set of ^{1}H NMR signals was observed in the spectrum of 23TAG, consistent with the formation of parallel-stranded G4 (Figure S8 B). Interestingly, the corresponding imino ^{1}H NMR signals were severely broadened upon addition of 0.5 mole equivalents of the **PL7**, while a few new signals were observed, consistent with formation of DNA-ligand complex(es). At equimolar mixture of DNA and **PL7** the signals for free 23TAG G4 were no longer observed. On the other hand, ^{1}H NMR signals corresponding to the complex(es) were observed for the samples prepared at 0.5–2.0 mole equivalents of the ligand, although they appeared broad and mostly unresolved at each

of the analyzed DNA:Ligand ratios. Notably, the relative intensities of the imino ^{1}H NMR signals for the complex(es) changed during titration. Hence, the NMR analysis suggests rather strong binding of the **PL7** to the parallel-stranded G4 adopted by 23TAG, which appeared to exhibit multiple sites amenable to the ligand interactions. It is interesting to note that the 'free' 23TAG parallel G4 formed under crowding conditions was no longer observed at 1 mole equivalent of **PL7**, while the 'free' hybrid analogue persisted even at 1:2 ratio between 23TAG and compound. These results are consistent with parallel G4 representing a better target for binding of **PL7**, whereby the interactions are aggravated by lateral loops in the hybrid topology, altogether stressing out the importance of the structural details related to the loops conformations with respect to the nearby (outer) G-quartets. The key role of residues extruded from the core of a G4 structure were further corroborated by the fact that shifting the equilibrium from parallel stranded G4 to complex formation required 1.5 mole equivalents of **PL7** in the case of CMA (*vide supra*) (Figure 4), while only 1 mole equivalent in case of 23TAG (Figure S8 B). This suggests that **PL7** exhibits higher binding affinity for parallel G4 formed by 23TAG than for parallel G4 formed by CMA. The differences may relate to the different DNA-ligand interactions at the interfaces between overhanging or loop residues and pendant groups of the tetra-substituted porphyrins. In particular, parallel G4 adopted by 23TAG exhibits three-residue propeller-type loops, while in the. case of CMA the propeller-type loops comprise only one or two residues. The longer loops in case of 23TAG with respect to CMA exhibit more flexibility, which potentially guides and facilitates binding of the **PL7**. Analogously, longer pendant groups of tetra-substituted porphyrins may promote G4 binding, which is substantiated by the results of comparative ^{1}H NMR.

Circular Dichroism

To further confirm the selectivity of **PL7** for the parallel topology, circular dichroism analyses were performed. As can be seen from Figure 6A, the spectrum of the CMA sequence showed a shape characteristic for parallel topology, with a positive band around 260 nm and a negative one at 240 nm. No changes in bands position were observed after either **TMPyP4** or **PL7** titrations, which confirmed the retention of the parallel topology (Figure 6A). The spectrum of free 23TAG (Figure 6B) showed a characteristic hybrid topology pattern, i.e., a positive band at 290 nm. Again, the G4 was subjected to titrations with 1.5 equivalents of **TMPyP4** or **PL7**: in contrast to CMA, with 23TAG there was a change in the spectra for both titrations, showing a decrease in the intensity of the band at 290 nm and an increase at 260 nm. This effect indicated further confirmation that porphyrin ligands show selectivity for parallel topology. If this was not present, as in the case of 23TAG, they stimulated refolding by activating structural equilibria. These underlay the failure to isolate the complex via NMR for the sequence with hybrid topology.

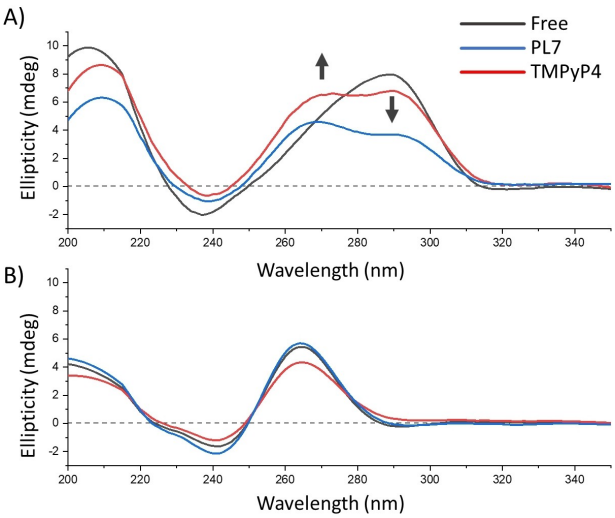

Figure 6. Circular dichroism spectra of (A) CMA and (B) 23TAG in diluted conditions. The spectra were recorded at 25 °C in 90%/10% $H_2O/^2H_2O$, at 20 mM KPi, pH 7.0- and 0.2-mM DNA. TMPyP4 and PL7 were added in 1.5 eq.

Mass Spectrometry

Mass spectrometry proves to be an efficient technique in assessing the stability of complexes formed by nucleic acids.[46] In our case, the analyses were conducted using a mass spectrometer with an ESI source, as reported in the experimental section. The primary advantage of electrospray ionization mass spectrometry is its capability to transfer analytes of interest from the sample solution to the mass spectrometer with minimal fragmentation. A common strategy for enhancing the ion response in ESI-MS is to add organic co-solvents that are more volatile than water, such as MeOH.[60] This phenomenon arises from the ability of methanol to reduce the surface tension of droplets, thereby promoting droplet formation, fission, and evaporation processes. As reported by Rosu *et al.*, the use of a specific methanol concentration not only results in a substantial increase in signal but also minimizes potential conformational alterations in solution.[46] Therefore, an 8:2 H_2O:MeOH solution was used to dilute stock solution to bring sequence concentration to 15 μM. The sequences employed for these experiments were 23TAG and CMT. CMT corresponds to CMA, with the distinction that in CMT, the second guanine has been replaced by thymine. As already reported,[44] NMR studies conducted on this sequence reveal that both the CMA and CMT G4 share common structural characteristics. These include a core comprised of three G-quartets, three propeller-type loops, and a T19 residue located at the 3′-end overhang. Since the fundamental folding topologies of the CMA and CMT G4 remain unaltered even when subjected to a single A–T nucleotide substitution at the 5′-end, CMT has been used for mass experiments instead of CMA. The stabilizing activity of **TMPyP4**, **PL7**, **PL7-Me** and **PL7-2Me** was evaluated by MS/MS using the collision-induced dissociation (CID) technique. The latter involves isolating the molecular ion in a collision chamber and gradually increasing the collision energy until the target peak

disappears. From these experiments, it was possible to calculate the energy required for dissociation of the complex peak to its relative half-intensity ($E_{COM}50\%$)[61] using the relative intensities of the target ions from Equation (1).

$$relative\ intensity = \frac{I_{Target\ Ion}}{I_{Target\ Ion} + I_{Dissociation\ Products}} \quad (1)$$

Mass spectrometry is less sensitive to structural equilibria than NMR spectroscopy making possible to isolate complexes with the 23TAG.

This supported the thesis that the reduction in intensity of the imino ^{1}H NMR signals observed during titrations of G4 with ligands was due to the formation of a complex. However, no Complex b at a G4:ligand ratio of 1:2 has been isolated, suggesting that one of the two terminal G-quartets of hybrid G4 is sterically hindered, impeding the stacking of the ligand. Complex b was isolated with CMT G4 using **TMPyP4** and **PL7**. Table 6 summarizes the results of the stability studies. Overall, the proposed ligands stabilized both CMT and 23TAG sequences. For CMT, both **PL7** and **TMPyP4** showed an increase in stability from Complex a to Complex b. Additionally, from the $E_{COM}50\%$ values, it is evident that an increase in the number of ligands present was proportional to an increase in G4 stability. However, it's important to note that this is not a trivial observation, as excessive ligand binding capacity can lead to destabilization and subsequent unfolding of the G4 structure.

Table 6. Gas phase stability of G4-porphyrin complexes calculated by collision induced dissociation experiments.

Oligonucleotide	Ligand	$E_{COM}50\%$ G4 (eV)
23TAG	No ligand	28.9
	TMPyP4[a]	38.5
	PL7[a]	38.8
	PL7-Me[a]	39.6
	PL7-2Me[a]	40.2
CMT	No ligand	26.5
	TMPyP4[a]	35.9
	TMPyP4[b]	48.5
	PL7[a]	35.9
	PL7[b]	45.5

Data were obtained by subjecting quadruplex samples and their respective complexes to MS/MS fragmentation. The quadruplexes were folded in a 0.2 mM solution of 100 mM tetramethyl ammonium acetate (TMAA) buffer at pH 7, containing 1 mM KCl. The solution was annealed at 60 °C for 30 seconds and then allowed to fold for 2 days. Further details are provided in the supplementary information. [a] Complex a with 1:1 stoichiometry. [b] Complex b with 1:2 stoichiometry.

Proliferation Assay

An MTT assay was conducted on MCF-7 cell lines, using **PL7** and **TMPyP4** porphyrins. The investigation aimed to assess the potential cytotoxic effects of these porphyrins on cancerous cell lines. The results (Figure 7) of the MTT assay unveiled a compelling dose-response relationship for both **PL7** and **TMPyP4**, revealing their impact on cell viability. Notably, **PL7** exhibited an IC_{50} value of $3.265 \pm 1.218\ \mu M$, indicating its potency in inhibiting cell proliferation. Also in this case, as for NMR experiments, results are comparable with once obtained for **TMPyP4**, that shows an IC_{50} of $3.651 \pm 1.197\ \mu M$. These findings showed that both molecules were able to induce a stop in the cell growth at relatively low concentrations.

Conclusions

A series of cationic porphyrins were designed and their interaction with different G4 s was evaluated. An initial molecular docking study identified the most promising ligands based on their interaction energies with G4 s of different nature and topology. The calculations showed parallel topology as

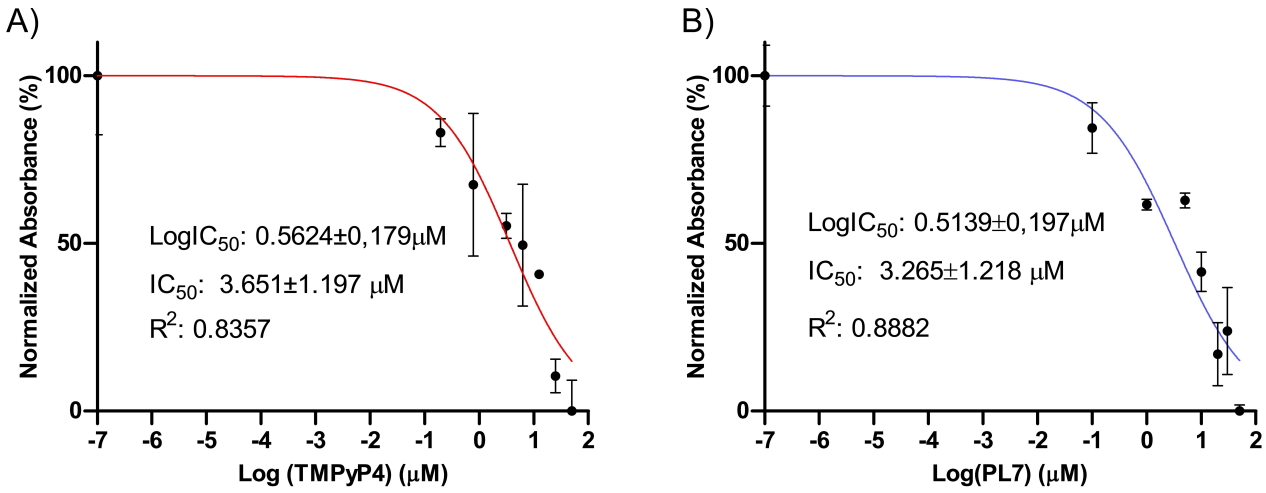

Figure 7. IC_{50} from the MTT assay on MCF-7 cell line with A) TMPyP4 and B) PL7. The x-axis represents the logarithm of the concentration while the y-axis contains the % of living cells in the sample. Each experiment was repeated 3 times, the results are presented as the mean, error bars represent ± the standard deviation

most preferred and **PL7** as the most promising derivative. In addiction **PL7** stabilizing ability was then evaluated by an extensive set of MD simulations of the telomeric parallel G4 in presence and absence of the ligand. The simulations were performed both at room temperature (300 K) and at higher temperature (500, 525 and 500 K) and indicated a stabilizing effect of **PL7** on the G4 structure. Considering these results, **PL7** and **TMPyP4** were synthesized, and binding constant evaluated on calf thymus (duplex), 23TAG (hybrid G4 from human telomeres) and CMA (parallel G4 from c-Myc) by UV-Visible titrations. While **TMPyP4** showed no selectivity, **PL7** showed a 3-fold preference for parallel G4 over duplex and hybrid G4. NMR spectroscopy was used to study the structures of the **PL7**/G4 complexes, again showing that the G4 CMA was preferred due to its topology. Circular dichroism analyses suggested that while in the case of all parallel G4 s there was no effect beyond coordination on the quartets, in the case of hybrid G4 s there was a structural change induced by the presence of the ligand, which drove it to refold in the parallel topology, triggering structural equilibria that did not allow NMR study. Molecular crowding conditions were tested on the 23TAG sequence to drive its folding in parallel topology. ^{1}H NMR-monitored titration of G4 with **PL7** showed appearance of a new set of signals consistent with the formation of DNA/ligand complex(es). The interaction of the amide groups with the loops of G4 was not identified by NMR, suggesting a dynamic coordination on the quartets. Analysis of the differences in imino ^{1}H NMR chemical shifts for CMA G4 in complexes with **PL7-Me** and **PL7-2Me** showed that the presence of at least one potential hydrogen bond donor in the ligand's pendant group balances the larger steric hindrance, which partially disfavors stacking on the quartets. Mass spectrometry collision-induced dissociation experiments on 23TAG and CMA complexes with **TMPyP4** and **PL7** have shown very similar stabilizing effects. Finally, preliminary cytotoxicity assays were performed on a breast cancer cell line in which the IC_{50} values obtained for **TMPyP4** and **PL7** were comparable. This study was able to confirm the propensity of porphyrin ligands for parallel G4, a topology preferred under the naturally occurring conditions of molecular crowding in the cellular environment. **PL7** demonstrated how the presence of amide groups gives a balance of steric hindrance and dipolar interaction with loops, that improves selectivity for parallel G4 s over other structures. Considering also the easy of synthesis, **PL7** could be regarded as a better alternative to **TMPyP4** in studies involving G4 binding.

Acknowledgements

FM acknowledges the National Supercomputer Center (Naiss) in Sweden for the computational resource and Fondazione Banco di Sardegna (FDS) (grant number F73C23001600007) for funding. Simone Mulliri, Elisabetta Cardinale and Fabio Esposito are kindly acknowledged for performing the docking for ligands PL6 and PL7. JP and MT thank the Slovenian Research and Innovation Agency [P1-0242, J1- 1704]. The authors would like to thank CERIC-ERIC consortium for the access to experimental facilities and financial support (grant No. 20232091). This work was financially supported by Regione Autonoma della Sardegna within the project "Green Chemistry" in "Drug Discovery: sintesi sostenibili di nuovi inibitori di telomerasi" (RASSR81788-Bando "Invito a presentare progetti di ricerca di base – Annualità 2017") Open Access publishing facilitated by Università degli Studi di Sassari, as part of the Wiley - CRUI-CARE agreement.

Conflict of Interests

The authors declare no conflict of interest.

Data Availability Statement

The data that support the findings of this study are available in the supplementary material of this article.

Keywords: DNA · G-quadruplexes · Molecular dynamics · Molecular recognition · NMR

[1] M. L. Bochman, K. Paeschke, V. A. Zakian, *Nat. Rev. Genet.* **2012**, *13*, 770–780.
[2] D. Yang in *G-Quadruplex Nucleic Acids: Methods and Protocols* (Eds: D. Yang, C. Lin), Springer New York, New York, NY **2019**, p. 3.
[3] L. Hayflick, P. S. Moorhead, *Exp. Cell Res.* **1961**, *25*, 585–621.
[4] A. G. Bodnar, M. Ouellette, M. Frolkis, S. E. Holt, C. P. Chiu, G. B. Morin, C. B. Harley, J. W. Shay, S. Lichtsteiner, W. E. Wright, *Science* **1998**, *279*, 349–352.
[5] J. W. Shay, W. E. Wright, *Semin. Cancer Biol.* **2011**, *21*, 349–353.
[6] N. W. Kim, M. A. Piatyszek, K. R. Prowse, C. B. Harley, M. D. West, P. L. C. Ho, G. M. Coviello, W. E. Wright, S. L. Weinrich, J. W. Shay, *Science* **1994**, *266*, 2011–2015.
[7] C. Bryan, C. Rice, H. Hoffman, M. Harkisheimer, M. Sweeney, E. Skordalakes, *Structure* **2015**, *23*, 1934–1942.
[8] A. Asai, Y. Oshima, Y. Yamamoto, T. Uochi, H. Kusaka, S. Akinaga, Y. Yamashita, K. Pongracz, R. Pruzan, E. Wunder, M. Piatyszek, S. Li, A. C. Chin, C. B. Harley, S. Gryaznov, *Cancer Res.* **2003**, *63*, 3931–3939.
[9] N. Kosiol, S. Juranek, P. Brossart, A. Heine, K. Paeschke, *Mol. Cancer* **2021**, *20*, 40.
[10] S. Balasubramanian, S. Neidle, *Curr. Opin. Chem. Biol.* **2009**, *13*, 345–353.
[11] C. Hennecker, L. Yamout, C. Zhang, C. Zhao, D. Hiraki, N. Moitessier, A. Mittermaier, *Int. J. Mol. Sci.* **2022**, *23*, 16020.
[12] S. Da Ros, G. Nicoletto, R. Rigo, S. Ceschi, E. Zorzan, M. Dacasto, M. Giantin, C. Sissi, *Int. J. Mol. Sci.* **2021**, *22*, 329.
[13] S. A. Miller, J. Nandi, N. E. Leadbeater, N. A. Eddy, *Eur. J. Org. Chem.* **2020**, *2020*, 108–112.
[14] V. González, L. H. Hurley, *Biochemistry* **2010**, *49*, 9706–9714.
[15] A. Siddiqui-Jain, C. L. Grand, D. J. Bearss, L. H. Hurley, *Proc. Natl. Acad. Sci. U. S. A.* **2002**, *99*, 11593–11598.
[16] J. Spiegel, S. Adhikari, S. Balasubramanian, *Trends Chem.* **2020**, *2*, 123–136.
[17] D. Miyoshi, N. Sugimoto, *Biochimie* **2008**, *90*, 1040–1051.
[18] B. Heddi, A. T. Phan, *J. Am. Chem. Soc.* **2011**, *133*, 9824–9833.
[19] T. Fujii, P. Podbevšek, J. Plavec, N. Sugimoto, *J. Inorg. Biochem.* **2017**, *166*, 190–198.
[20] V. Viglasky, T. Hianik, *Gen. Physiol. Biophys.* **2013**, *32*, 149–172.
[21] T. Troha, I. Drevenšek-Olenik, M. Webba da Silva, L. Spindler, *Langmuir* **2016**, *32*, 7056–7063.
[22] F. C. Simmel, W. U. Dittmer, *Small* **2005**, *1*, 284–299.
[23] K. Shin-ya, K. Wierzba, K. Matsuo, T. Ohtani, Y. Yamada, K. Furihata, Y. Hayakawa, H. Seto, *J. Am. Chem. Soc.* **2001**, *123*, 1262–1263.
[24] S. M. Gowan, J. R. Harrison, L. Patterson, M. Valenti, M. A. Read, S. Neidle, L. R. Kelland, *Mol. Pharmacol.* **2002**, *61*, 1154–1162.

[25] W. J. Chung, B. Heddi, M. Tera, K. Iida, K. Nagasawa, A. T. Phan, *J. Am. Chem. Soc.* **2013**, *135*, 13495–13501.
[26] F. Hamon, E. Largy, A. Guédin-Beaurepaire, M. Rouchon-Dagois, A. Sidibe, D. Monchaud, J.-L. Mergny, J.-F. Riou, C.-H. Nguyen, M.-P. Teulade-Fichou, *Angew. Chem. Int. Ed.* **2011**, *50*, 8745–8749.
[27] S. Balasubramanian, L. H. Hurley, S. Neidle, *Nat. Rev. Drug Discov.* **2011**, *10*, 261–275.
[28] A. De Cian, E. DeLemos, J.-L. Mergny, M.-P. Teulade-Fichou, D. Monchaud, *J. Am. Chem. Soc.* **2007**, *129*, 1856–1857.
[29] A. Terenzi, H. Gattuso, A. Spinello, B. K. Keppler, C. Chipot, F. Dehez, G. Barone, A. Monari, *Antioxidants (Basel)* **2019**, *8*, 472.
[30] A. Criscuolo, E. Napolitano, C. Riccardi, D. Musumeci, C. Platella, D. Montesarchio, *Pharmaceutics* **2022**, *14*, 2361.
[31] S. Asamitsu, S. Obata, Z. Yu, T. Bando, H. Sugiyama, *Molecules* **2019**, *24*, 429.
[32] S. Pelliccia, J. Amato, D. Capasso, S. Di Gaetano, A. Massarotti, M. Piccolo, C. Irace, G. C. Tron, B. Pagano, A. Randazzo, E. Novellino, M. Giustiniano, *J. Med. Chem.* **2020**, *63*, 2035–2050.
[33] V. Pirota, M. Stasi, A. Benassi, F. Doria, in *Annual Reports in Medicinal Chemistry*, (Ed: S. Neidle), Academic Press, **2020**, pp. 163–196.
[34] M. Ghahremani Nasab, L. Hassani, S. Mohammadi Nejad, D. Norouzi, *J. Biol. Phys.* **2017**, *43*, 5–14.
[35] R. T. Wheelhouse, D. Sun, H. Han, F. X. Han, L. H. Hurley, *J. Am. Chem. Soc.* **1998**, *120*, 3261–3262.
[36] C. L. Grand, H. Han, R. M. Muñoz, S. Weitman, D. D. Von Hoff, L. H. Hurley, D. J. Bearss, *Mol. Cancer Ther.* **2002**, *1*, 565–573.
[37] J. Ren, J. B. Chaires, *Biochemistry* **1999**, *38*, 16067–16075.
[38] I. M. Dixon, F. Lopez, J.-P. Estève, A. M. Tejera, M. A. Blasco, G. Pratviel, B. Meunier, *ChemBioChem* **2005**, *6*, 123–132.
[39] I. M. Dixon, F. Lopez, A. M. Tejera, J.-P. Estève, M. A. Blasco, G. Pratviel, B. Meunier, *J. Am. Chem. Soc.* **2007**, *129*, 1502–1503.
[40] Y. Du, D. Zhang, W. Chen, M. Zhang, Y. Zhou, X. Zhou, *Bioorg. Med. Chem.* **2010**, *18*, 1111–1116.
[41] A. Ferino, G. Nicoletto, F. D'Este, S. Zorzet, S. Lago, S. N. Richter, A. Tikhomirov, A. Shchekotikhin, L. E. Xodo, *J. Med. Chem.* **2020**, *63*, 1245–1260.
[42] G. N. Parkinson, M. P. H. Lee, S. Neidle, *Nature* **2002**, *417*, 876–880.
[43] A. Ambrus, D. Chen, J. Dai, R. A. Jones, D. Yang, *Biochemistry* **2005**, *44*, 2048–2058.
[44] M. Trajkovski, E. Morel, F. Hamon, S. Bombard, M.-P. Teulade-Fichou, J. Plavec, *Chem. – Eur. J.* **2015**, *21*, 7798–7807.
[45] M. Adrian, B. Heddi, A. T. Phan, *Methods* **2012**, *57*, 11–24.
[46] F. Rosu, E. De Pauw, V. Gabelica, *Biochimie* **2008**, *90*, 1074–1087.
[47] G. Ribaudo, A. Ongaro, G. Zagotto, M. Memo, A. Gianoncelli, *Nat. Prod. Res.* **2021**, *35*, 2583–2587.
[48] V. Gabelica, *Acc. Chem. Res.* **2021**, *54*, 3691–3699.
[49] R. Day, B. J. Bennion, S. Ham, V. Daggett, *J. Mol. Biol.* **2002**, *322*, 189–203.
[50] D. O. Alonso, E. Alm, V. Daggett, *Structure* **2000**, *8*, 101–110.
[51] G. Todde, S. Hovmöller, A. Laaksonen, F. Mocci, *Proteins Struct. Funct. Bioinforma.* **2014**, *82*, 2353–2363.
[52] S. Mulliri, A. Laaksonen, P. Spanu, R. Farris, M. Farci, F. Mingoia, G. N. Roviello, F. Mocci, *Int. J. Mol. Sci.* **2021**, *22*, 6028.
[53] A. T. Phan, V. Kuryavyi, K. N. Luu, D. J. Patel, *Nucleic Acids Res.* **2007**, *35*, 6517–6525.
[54] K. N. Luu, A. T. Phan, V. Kuryavyi, L. Lacroix, D. J. Patel, *J. Am. Chem. Soc.* **2006**, *128*, 9963–9970.
[55] R. I. Mathad, E. Hatzakis, J. Dai, D. Yang, *Nucleic Acids Res.* **2011**, *39*, 9023–9033.
[56] T. Santos, J. Lopes-Nunes, D. Alexandre, A. Miranda, J. Figueiredo, M. S. Silva, J.-L. Mergny, C. Cruz, *Biochimie* **2022**, *200*, 8–18.
[57] C. Wei, J. Wang, M. Zhang, *Biophys. Chem.* **2010**, *148*, 51–55.
[58] R. I. Mathad, E. Hatzakis, J. Dai, D. Yang, *Nucleic Acids Res.* **2011**, *39*, 9023–9033.
[59] A. T. Phan, V. Kuryavyi, K. N. Luu, D. J. Patel, *Nucleic Acids Res.* **2007**, *35*, 6517–6525.
[60] R. Ferreira, A. Marchand, V. Gabelica, *Methods* **2012**, *57*, 56–63.
[61] M. Torvinen, E. Kalenius, F. Sansone, A. Casnati, J. Jänis, *J. Am. Soc. Mass Spectrom.* **2012**, *23*, 359–365.
[62] "Computational Platform for Molecular Discovery & Design," can be found under https://www.schrodinger.com/platform/ (accessed 2024–04-15).
[63] "Life Science: Maestro," can be found under https://www.schrodinger.com/platform/products/maestro/ (accessed 2024–04-15).
[64] "2D Sketcher," can be found under https://www.schrodinger.com/platform/products/schrodinger-2d-sketcher/ (accessed 2024–04-15).
[65] "Schrödinger Release 2024–1: LigPrep, Schrödinger, LLC, New York, NY, 2024.," can be found under https://www.schrodinger.com/platform/products/ligprep/ (accessed 2024–04-15).
[66] J. Dai, M. Carver, C. Punchihewa, R. A. Jones, D. Yang, *Nucleic Acids Res.* **2007**, *35*, 4927–4940.
[67] Y. Wang, D. J. Patel, *Structure* **1993**, *1*, 263–282.
[68] J. C. Shelley, A. Cholleti, L. L. Frye, J. R. Greenwood, M. R. Timlin, M. Uchimaya, *J. Comput. Aided Mol. Des.* **2007**, *21*, 681–691.
[69] E. Harder, W. Damm, J. Maple, C. Wu, M. Reboul, J. Y. Xiang, L. Wang, D. Lupyan, M. K. Dahlgren, J. L. Knight, J. W. Kaus, D. S. Cerutti, G. Krilov, W. L. Jorgensen, R. Abel, R. A. Friesner, *J. Chem. Theory Comput.* **2016**, *12*, 281–296.
[70] W. L. Jorgensen, D. S. Maxwell, J. Tirado-Rives, *J. Am. Chem. Soc.* **1996**, *118*, 11225–11236.
[71] R. A. Friesner, J. L. Banks, R. B. Murphy, T. A. Halgren, J. J. Klicic, D. T. Mainz, M. P. Repasky, E. H. Knoll, M. Shelley, J. K. Perry, D. E. Shaw, P. Francis, P. S. Shenkin, *J. Med. Chem.* **2004**, *47*, 1739–1749.
[72] T. A. Halgren, R. B. Murphy, R. A. Friesner, H. S. Beard, L. L. Frye, W. T. Pollard, J. L. Banks, *J. Med. Chem.* **2004**, *47*, 1750–1759.
[73] R. A. Friesner, R. B. Murphy, M. P. Repasky, L. L. Frye, J. R. Greenwood, T. A. Halgren, P. C. Sanschagrin, D. T. Mainz, *J. Med. Chem.* **2006**, *49*, 6177–6196.
[74] R. Galindo-Murillo, J. C. Robertson, M. Zgarbová, J. Šponer, M. Otyepka, P. Jurečka, T. E. I. Cheatham, *J. Chem. Theory Comput.* **2016**, *12*, 4114–4127.
[75] J. Šponer, G. Bussi, P. Stadlbauer, P. Kührová, P. Banáš, B. Islam, S. Haider, S. Neidle, M. Otyepka, *Biochim. Biophys. Acta Gen. Subj.* **2017**, *1861*, 1246–1263.
[76] A. Atzori, S. Liggi, A. Laaksonen, M. Porcu, A. P. Lyubartsev, G. Saba, F. Mocci, *Can. J. Chem.* **2016**, *94*, 1181–1188.
[77] M. Havrila, P. Stadlbauer, B. Islam, M. Otyepka, J. Šponer, *J. Chem. Theory Comput.* **2017**, *13*, 3911–3926.
[78] F. Mocci, A. Laaksonen, *Soft Matter* **2012**, *8*, 9268–9284.
[79] M. Rebič, A. Laaksonen, J. Šponer, J. Uličný, F. Mocci, *J. Phys. Chem. B* **2016**, *120*, 7380–7391.
[80] M. Krepl, M. Zgarbová, P. Stadlbauer, M. Otyepka, P. Banáš, J. Koča, T. E. Cheatham, P. Jurečka, J. Sponer, *J. Chem. Theory Comput.* **2012**, *8*, 2506–2520.
[81] M. Zgarbová, J. Šponer, M. Otyepka, T. E. Cheatham, R. Galindo-Murillo, P. Jurečka, *J. Chem. Theory Comput.* **2015**, *11*, 5723–5736.
[82] A. Pérez, I. Marchán, D. Svozil, J. Sponer, T. E. Cheatham, C. A. Laughton, M. Orozco, *Biophys. J.* **2007**, *92*, 3817–3829.
[83] M. Zgarbová, F. J. Luque, J. Šponer, T. E. Cheatham, M. Otyepka, P. Jurečka, *J. Chem. Theory Comput.* **2013**, *9*, 2339–2354.
[84] W. D. Cornell, P. Cieplak, C. I. Bayly, I. R. Gould, K. M. Merz, D. M. Ferguson, D. C. Spellmeyer, T. Fox, J. W. Caldwell, P. A. Kollman, *J. Am. Chem. Soc.* **1995**, *117*, 5179–5197.
[85] J. Wang, W. Wang, P. A. Kollman, D. A. Case, *J. Mol. Graph. Model.* **2006**, *25*, 247–260.
[86] I. Rajasingh, B. Rajan, R. S. Rajan, *Appl. Math.* **2010**, *01*, 499–503.
[87] C. Komenan, *Adv. Lit. Study* **2019**, *07*, 176–192.
[88] E. Görg, *Adv. Hist. Stud.* **2014**, *03*, 56–67.
[89] M. R. Farahani, W. Gao, *Appl. Math.* **2015**, *06*, 2319–2325.
[90] F. G. Alvarenga, M. J. S. Houndjo, A. V. Monwanou, J. B. C. Orou, *J. Mod. Phys.* **2013**, *04*, 130–139.
[91] C. I. Bayly, P. Cieplak, W. Cornell, P. A. Kollman, *J. Phys. Chem.* **1993**, *97*, 10269–10280.
[92] J. Wang, R. M. Wolf, J. W. Caldwell, P. A. Kollman, D. A. Case, *J. Comput. Chem.* **2004**, *25*, 1157–1174.
[93] H. J. C. Berendsen, J. R. Grigera, T. P. Straatsma, *J. Phys. Chem.* **1987**, *91*, 6269–6271.
[94] I. S. Joung, T. E. I. Cheatham, *J. Phys. Chem. B* **2009**, *113*, 13279–13290.
[95] I. S. Joung, T. E. I. Cheatham, *J. Phys. Chem. B* **2008**, *112*, 9020–9041.
[96] R. Salomon-Ferrer, D. A. Case, R. C. Walker, *WIREs Comput. Mol. Sci.* **2013**, *3*, 198–210.
[97] D. A. Case, T. E. Cheatham, T. Darden, H. Gohlke, R. Luo, K. M. Merz, A. Onufriev, C. Simmerling, B. Wang, R. J. Woods, *J. Comput. Chem.* **2005**, *26*, 1668–1688.
[98] D. A. Pearlman, D. A. Case, J. W. Caldwell, W. S. Ross, T. E. Cheatham, S. DeBolt, D. Ferguson, G. Seibel, P. Kollman, *Comput. Phys. Commun.* **1995**, *91*, 1–41.
[99] H. J. C. Berendsen, J. P. M. Postma, W. F. van Gunsteren, J. Hermans, in *Intermolecular Forces Proc. Fourteenth Jerus. Symp. Quantum Chem.*

Biochem. Held Jerus. Isr. April 13–16 1981 (Ed.: B. Pullman), Springer Netherlands, Dordrecht, **1981**, 331–342.
[100] J.-P. Ryckaert, G. Ciccotti, H. J. C. Berendsen, *J. Comput. Phys.* **1977**, *23*, 327–341.
[101] T. Darden, D. York, L. Pedersen, *J. Chem. Phys.* **1993**, *98*, 10089–10092.
[102] G. Todde, S. Hovmöller, A. Laaksonen, F. Mocci, *Proteins* **2014**, *82*, 2353–2363.
[103] R. Day, B. J. Bennion, S. Ham, V. Daggett, *J. Mol. Biol.* **2002**, *322*, 189–203.
[104] D. O. Alonso, E. Alm, V. Daggett, *Struct. Lond. Engl. 1993* **2000**, *8*, 101–110.
[105] G. Magdy, F. Belal, A. F. Abdel Hakiem, A. M. Abdel-Megied, *Int. J. Biol. Macromol.* **2021**, *182*, 1852–1862.
[106] A. S. Levenson, V. C. Jordan, *Cancer Res.* **1997**, *57*, 3071–3078.
[107] T. Mosmann, *J. Immunol. Methods* **1983**, *65*, 55–63.

Manuscript received: July 9, 2024
Accepted manuscript online: September 18, 2024
Version of record online: ■■, ■■

RESEARCH ARTICLE

Molecular docking and dynamics and multiple spectroscopic and spectrometric determinations allowed us to monitor interaction with different DNA sequences of simple cationic porphyrins. 5,10,15,20-tetrakis-(1-acetamido-4-pyridyl)porphyrin bromide in particular demonstrated a better selectivity compared to tetramethylpyridylporphyrin in binding G-quadruplex with parallel topology compared with hybrid and with duplex forming oligonucleotides.

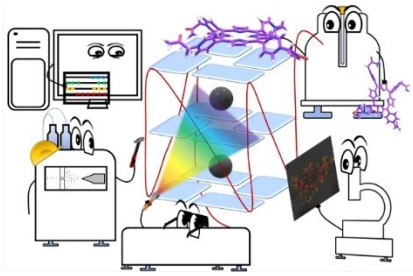

G. Satta, M. Trajkovski, A. Cantara, M. Mura, C. Meloni, G. Olla, M. Dobrovolná, L. Pisano, S. Gaspa, A. Salis, L. De Luca, F. Mocci, V. Brazda, J. Plavec, M. Carraro**